

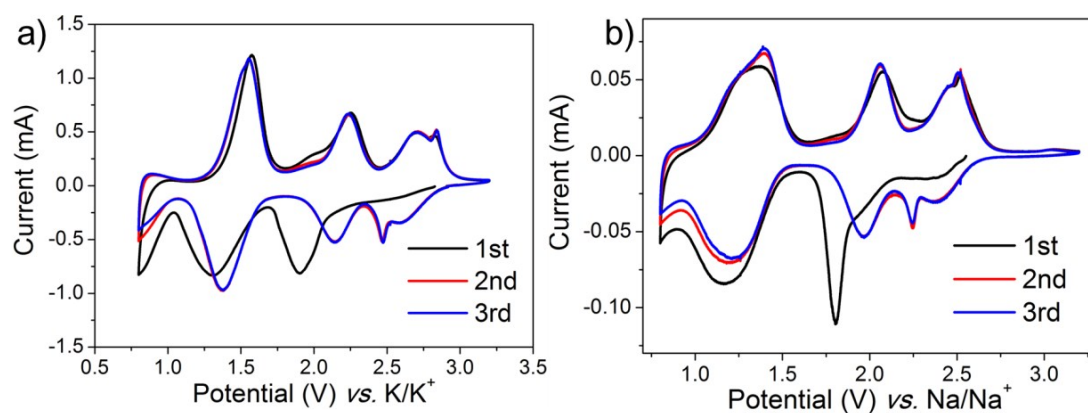
## Supporting Information

### An Organic Cathode with High Capacities for Fast-Charge Potassium-Ion Batteries

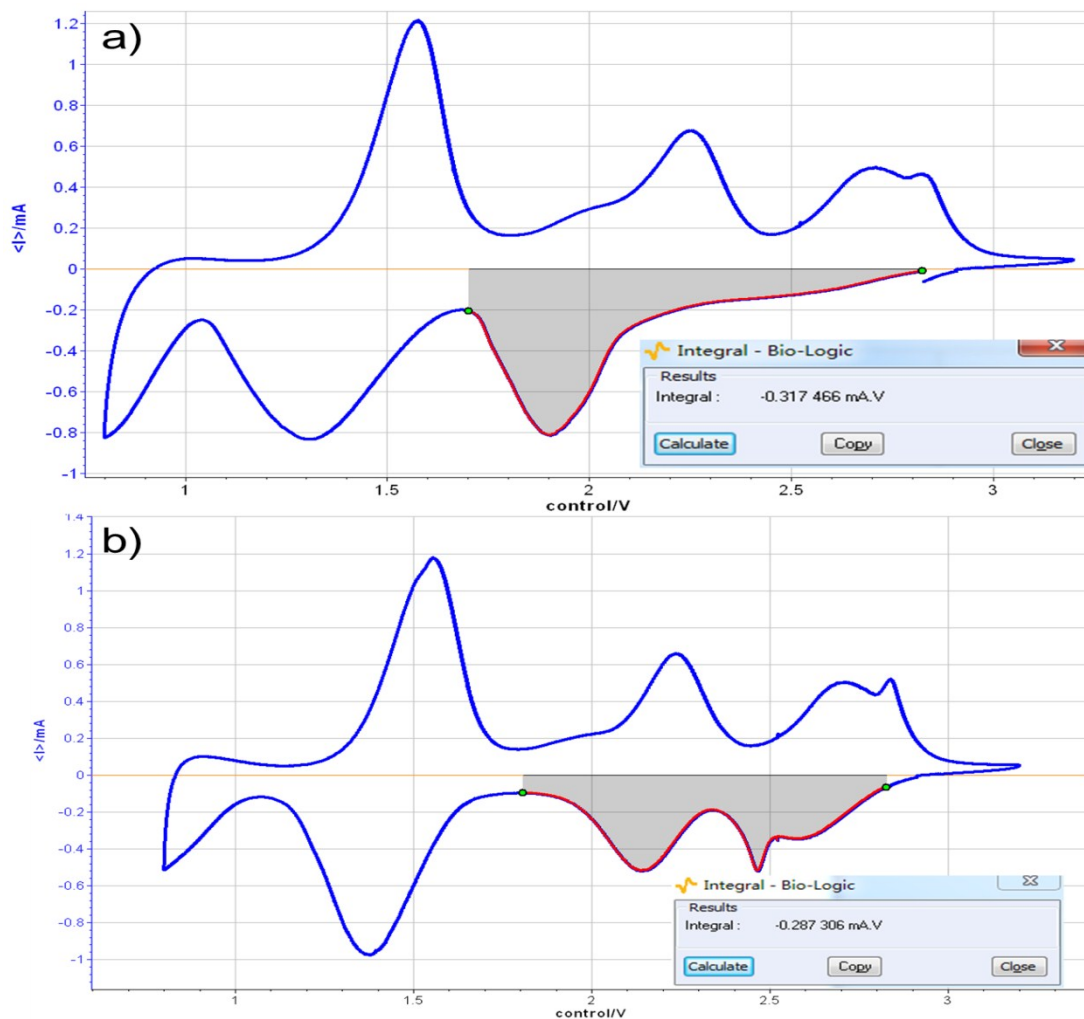
Mi Tang, Yanchao Wu, Yuan Chen, Cheng Jiang, Shaolong Zhu, Shuming Zhuo and  
Chengliang Wang\*

School of Optical and Electronic Information, Wuhan National Laboratory for  
Optoelectronics (WNLO), Huazhong University of Science and Technology, Wuhan  
430074, China.

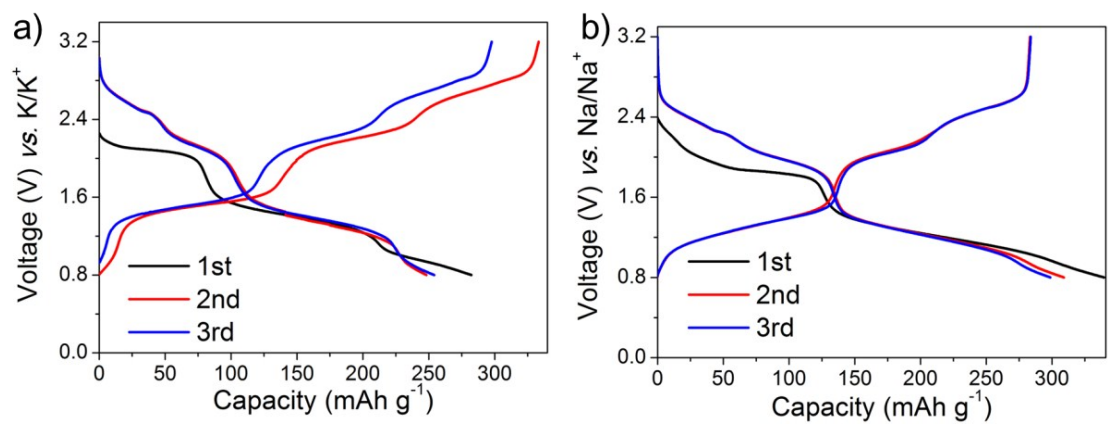
Email: [clwang@hust.edu.cn](mailto:clwang@hust.edu.cn)



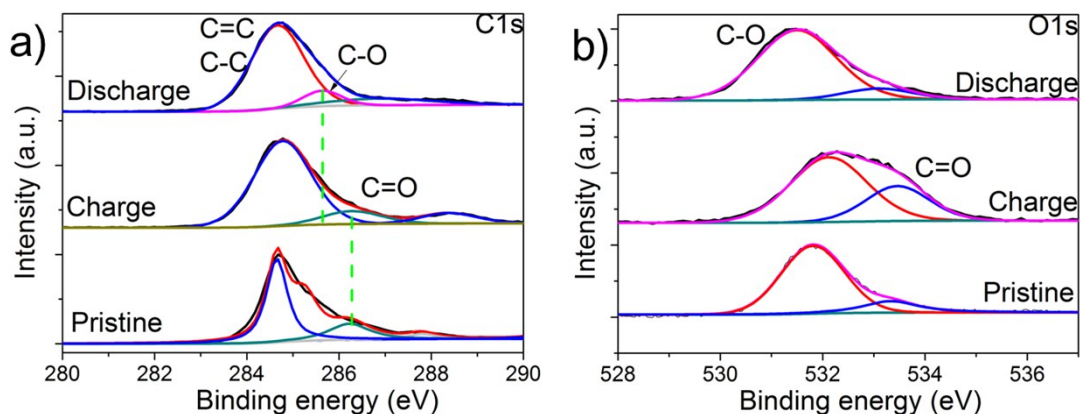
**Figure S1.** The CV curves of PPTS electrodes in a) K-ion and b) Na-ion batteries. All the shapes and current densities of every redox pairs are quite similar, suggesting the same electrochemical storage mechanism as shown in Figure 1A for K-ion batteries. The electrode potential of every peak is about 0.2 V higher for PIBs than those in SIBs. The higher potentials of PPTS electrodes in PIBs are owing to the lower electrode potential of K/K<sup>+</sup> than that of Na/Na<sup>+</sup> and would benefit the high power density.



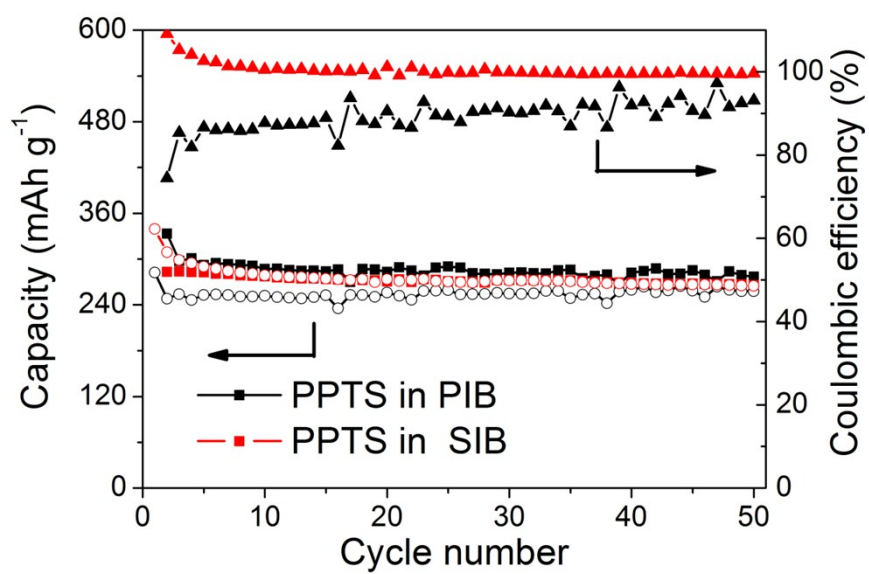
**Figure S2.** The CV integrals of the peaks around 2 V. a) The first scan and b) the second scan of PPTS in PIBs. Similarly with PPTS in SIBs, the electron transfer number is almost the same between 1.8-2.8 V in the first and the second cathodic scan for PPTS electrodes, suggesting the same mechanism during the first and the second scan in this area and the structural stability of PPTS. These results suggested that the difference between the first and subsequent cathodic scans can probably be attributed to the activation process, which needs a higher potential for relaxation of the strain/stress in the first scan (lower voltage compared with the subsequent cycles).<sup>1</sup>



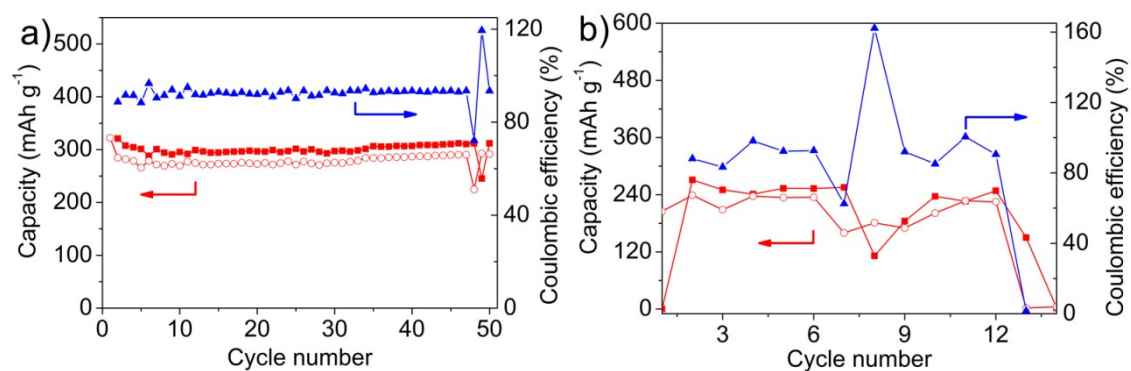
**Figure S3.** The contrastive electrochemical performance of PPTS at a current density of 100 mA g<sup>-1</sup>. a) PPTS in PIBs; b) PPTS in SIBs.



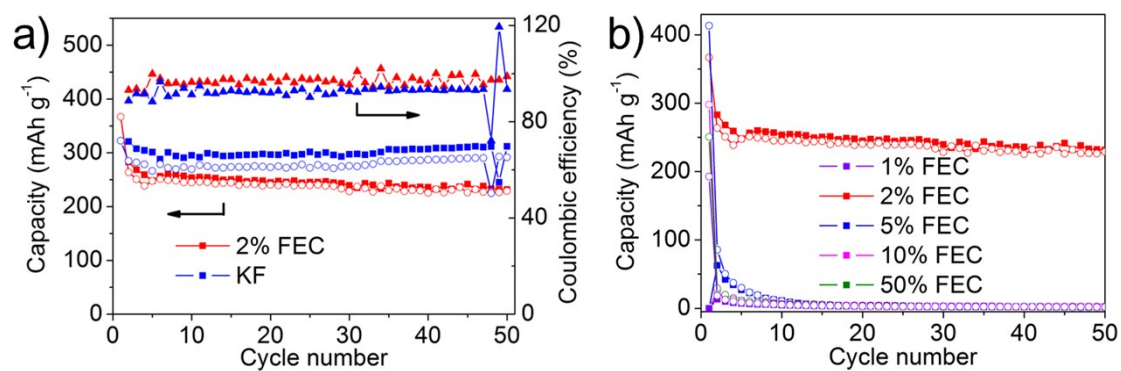
**Figure S4.** The ex-situ X-ray photoelectron spectroscopy (XPS) of PPTS electrodes. a) The peak intensity of C=O located at  $\sim 286.2$  eV decreased with increase of C-O ( $\sim 285.6$  eV) in the C1s spectra after discharging, indicating the reduction of C=O into C-O and the potassiation during discharging. And upon being recharged, the peak intensity of C=O recovered reversibly. b) Similarly, the reversible transformation from C=O (532.7 eV) to C-O bonds (531.8 eV) can be reconfirmed by the O1s spectra. This reversible transformation between C=O and C-O bonds during charge and discharge cycles is coincident with the theoretical storage mechanism.



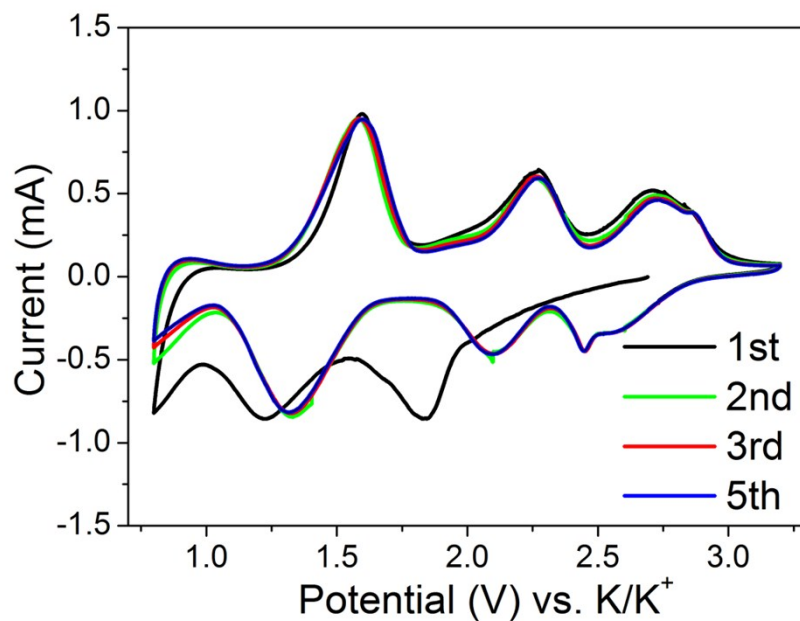
**Figure S5.** Comparisons of the specific capacity and Coulombic efficiency of PPTS in PIBs and SIBs at current density of 100 mA g<sup>-1</sup>.



**Figure S6.** Different electrolyte additives were used to improve the CE of PPTS-K cells at current density of 100 mA g<sup>-1</sup>: a) by adding saturated KF solution in DME as additives (50%, v/v). The addition of KF indeed improve the CE from 90 to 93%; however, the cells became not stable after tens cycles. b) by adding saturated KNO<sub>3</sub> solution in DME as additives (50%, v/v). The addition of KNO<sub>3</sub> resulted in unstable capacities and CE. It should be noted different from the situation of LiF and LiNO<sub>3</sub> in lithium-ion batteries, the solubility of KF and KNO<sub>3</sub> in DME are much lower, the instability may also be originated from the precipitation of the additives during cycling.

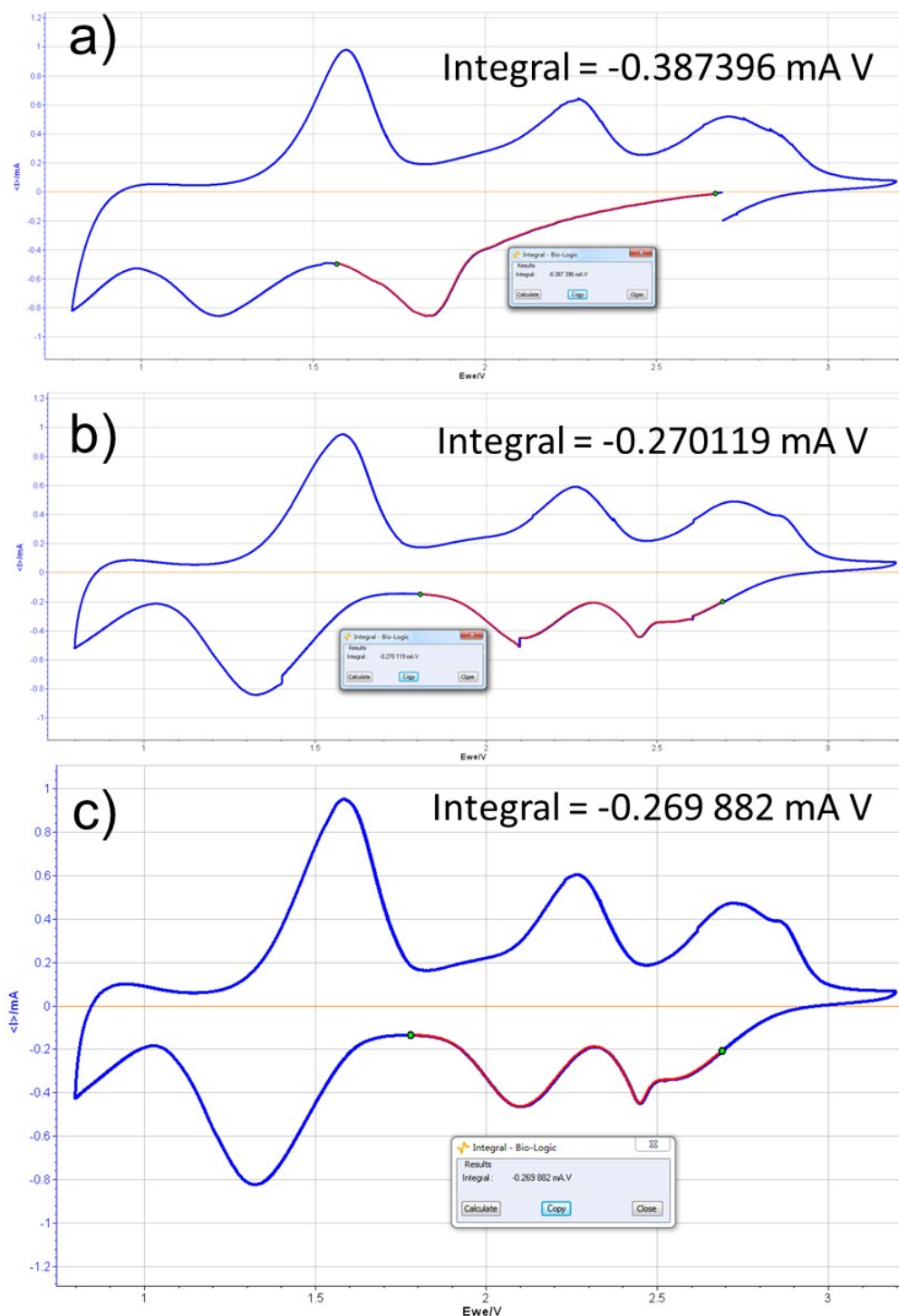


**Figure S7.** Comparisons of the specific capacity and Coulombic efficiency at current density of 100 mA g<sup>-1</sup>. a) The Coulombic efficiency with two kinds of additives: 2% FEC (red) and KF saturated solution of DME (blue). It is clear that although the addition of KF can maintain the higher capacity, the CE and the stability were lower than those with addition of FEC. b) Different ratio of FEC were added into 1.0 M KPF<sub>6</sub> in DME.

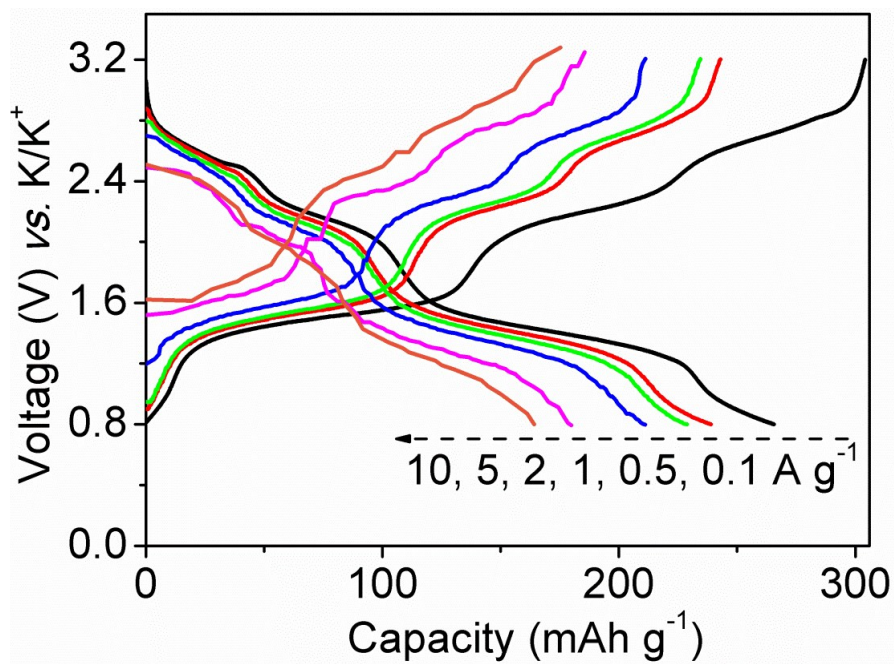


**Figure S8.** The CV curves of the PPTS electrode by using 1 M KPF<sub>6</sub> in DME as electrolyte with addition of 2% FEC measured at 0.5 mV s<sup>-1</sup> between 0.8 V and 3.2 V. The CV curves are quite similar with those cycled in the electrolyte without addition of FEC. The increase (compared with the samples without FEC) of peak intensity at around 2 V in the first cycle can probably be ascribed to the decomposition of FEC (Figure S5).

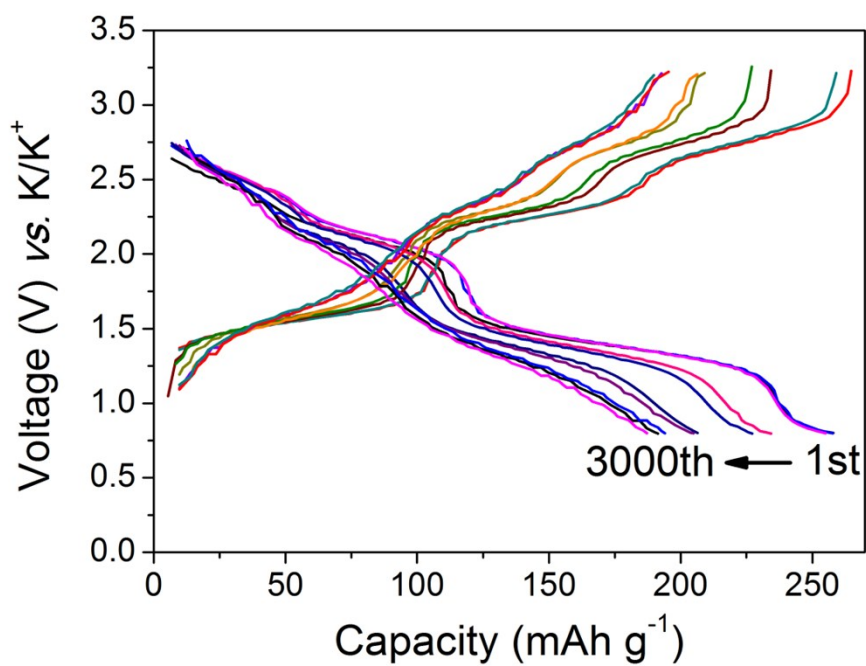




**Figure S9.** The CV integrals of the peaks around 2 V by using 1 M  $\text{KPF}_6$  in DME as electrolyte with addition of 2% FEC. a) The first scan, b) the second scan and c) the third scan of PPTS in PIBs. The increase of peak intensity at around 2 V in the first cycle can probably be ascribed to the decomposition of FEC. The shape and the current density kept stable afterwards, suggesting the reversibility of PPTS.

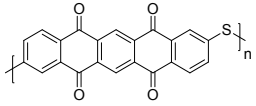
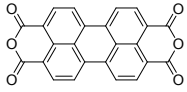
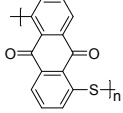


**Figure S10.** Voltage profiles of PPTS electrodes for rate performance by using 1 M KPF<sub>6</sub> in DME as electrolyte without addition of FEC.



**Figure S11.** Representative charge and discharge profiles at a current density of 5 A g<sup>-1</sup> by using 1 M KPF<sub>6</sub> in DME as electrolyte without addition of FEC.

**Table S1.** Comparison of representative cathode materials in potassium-ion batteries

Materials	Content of active materials (conductive additives, binder)	Low-rate capacity, mAh/g (current density, mA/g)	High-rate capacity, mAh/g (current density, mA/g)	Reversible capacity, cycles (current density, mA/g)	Discharge plateau (V)	Ref.
 PPTS	50% (SP, CMC-Na)	260 (100)	163 (10000)	190, 3000 (5000)	2.8~1.2	This work
 PTCDA	70% (SP, PVDF)	131 (10)	88 (200)	117, 200 (50)	2.4~2.2	2
 PAQS	70% (SP, PVDF)	200 (20)	68 (200)	190, 50 (20)	2.3~1.6	3
$K_2(CO)_6$	60% (SP, PVDF)	210 (100)	164 (2000)	130, 100 (200)	2.5~1.2	4
$K_3V_2(PO_4)_3$	80% (SP, PVDF)	54 (20)	20 (200)	52, 100 (20)	3.9~3.6	5
$K_xMnFe(CN)_6$ ( $0 \leq x \leq 2$ )	60% (CB, CMC-Na)	142 (31)	97 (312)	100, 100 (156)	4.0~3.6	6
$K_{0.6}CoO_2$	80% (SP, PTFE)	80 (2)	43 (150)	40, 120 (100)	~2.7	7
$K_{0.3}MnO_2$	85% (CB, PVDF)	70 (27.9)	54 (2790)	65, 685 (27.9)	~3.0	8
$K_{1.92}Fe[Fe(CN)_6]_{0.94} \cdot 0.5H_2O$	70% (CB, PVDF)	130 (65)	100 (1300)	133, 200 (65)	3.7 3.0	9
$KVPO_4F$	70% (AB, PVDF)	92 (6.65)	65 (665)	70, 50 (6.65)	4.1	10
$KFe[Fe(CN)_6]$	electro-deposition	78 (8.7)	not given	70, 500 (8.7)	3.8	11

Note: SP: carbon Super; KB: Ketjen black; CB: carbon black; PVDF: polyvinylidene fluoride; PTFE: poly(tetrafluoroethylene); AB: acetylene black.

**Table S2.** Slopes of every peak in the log *i* vs. log *v* plots in Figure 4B

Peak		1	2	3
<i>b</i> -value	A	0.80	0.84	0.92
	C	0.84	0.87	0.91

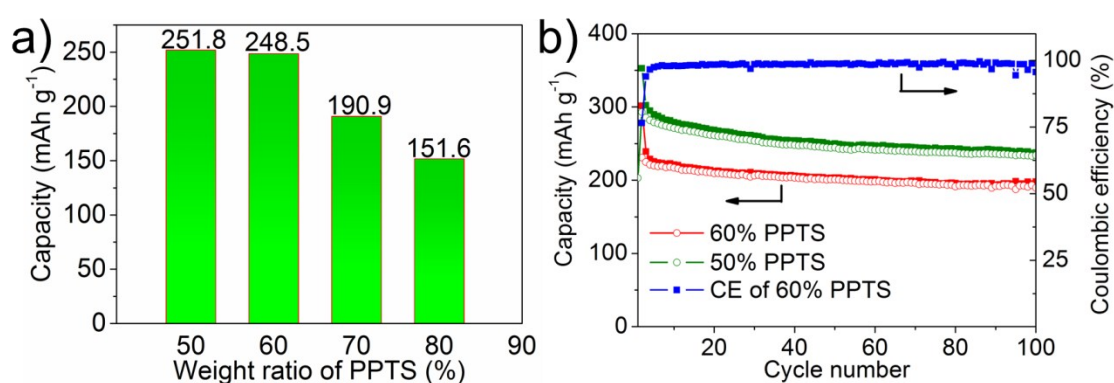


**Figure S12.** The electrochemical performance by using different ratio of active materials. a) Capacity comparison of PPTS electrodes by using different ratios of active materials at a current density of 100 mA g<sup>-1</sup>. b) Comparisons of the specific capacity and cycle stability with two ratios of conductive additives: 60% (red) and 50% (olive) at a current density of 1000 mA g<sup>-1</sup>. PPTS-based cells delivered a capacity of about 248.5 mAh g<sup>-1</sup> by using of 30 wt% of Super P (corresponding to 60 wt% of active materials), at a current density of 100 mA g<sup>-1</sup>. This capacity is quite close to that using 40 wt% of Super P (corresponding to 50 wt% of active materials). However, at a current density of 1000 mA g<sup>-1</sup>, the capacity significantly reduced by ~40 mAh g<sup>-1</sup>. Further reducing the content of Super P will lead to higher capacity degradation. The capacity degradation is probably due to the poor electric conductivity of organic materials. This problem may be solved by using composites with highly conductive carbon materials, nanocomposites etc., which have been widely studied in both organic and inorganic electrodes.<sup>5, 12, 13</sup>

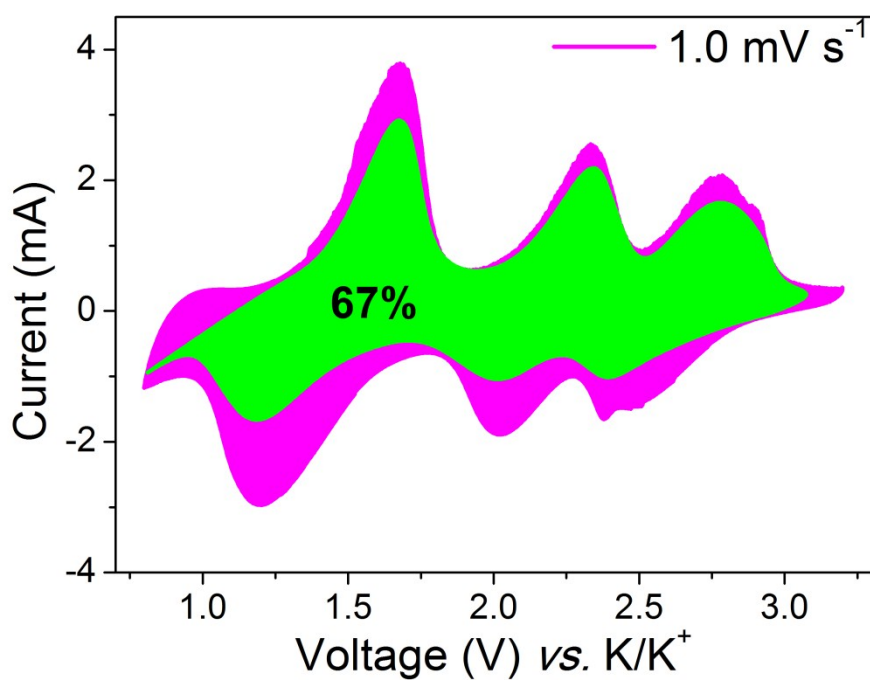


**Figure S13.** Capacity contribution at scan rate of  $1 \text{ mV s}^{-1}$ , showing high contribution of the capacitive process rather than a diffusion-controlled process. The specific capacity is much larger than the typical EDLC, suggesting that the capacitive contribution is dominated by an intercalation mechanism. The capacitive effect is probably due to the layer-by-layer stacking of PPTS, which facilitates the ionic transport, as reported in our previous paper.

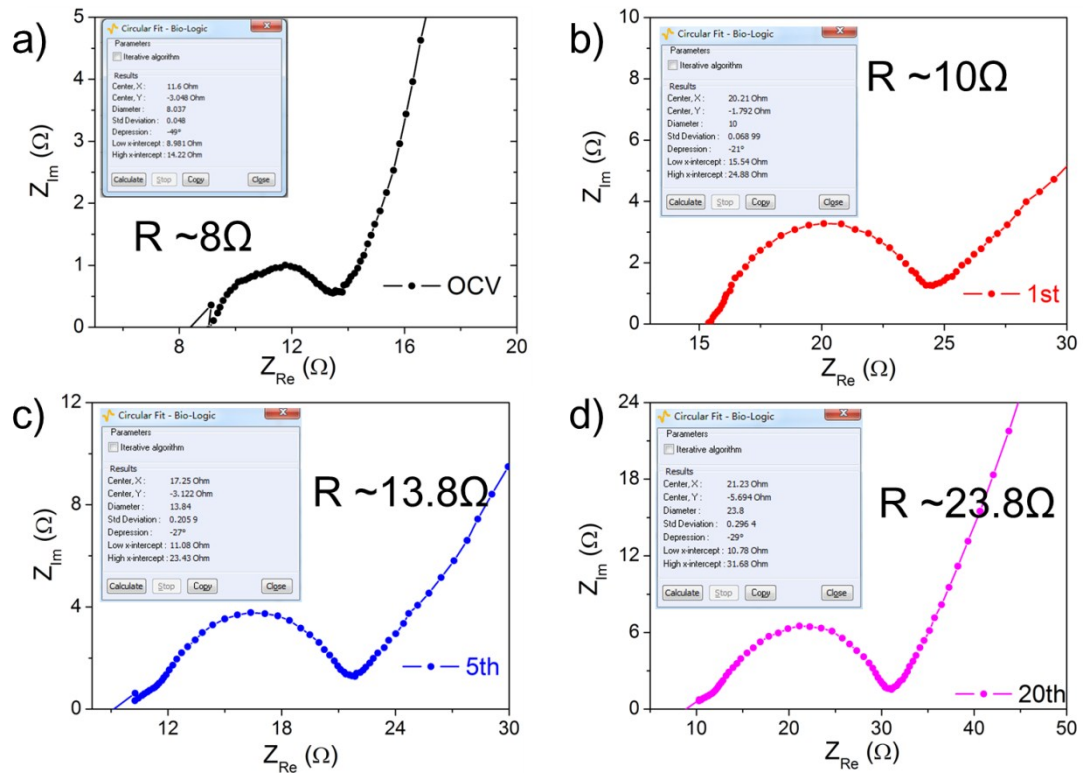


**Figure S14.** The Nyquist plot of PPTS electrode during cycling at a current density of  $1 \text{ A g}^{-1}$ : a) open-circuit voltage (OCV); after being discharged b) 1 cycle; c) 5 cycles and d) 20 cycles. Slight increase of charge-transfer resistance possibly can be attributed to the formation of SEI after cycling.

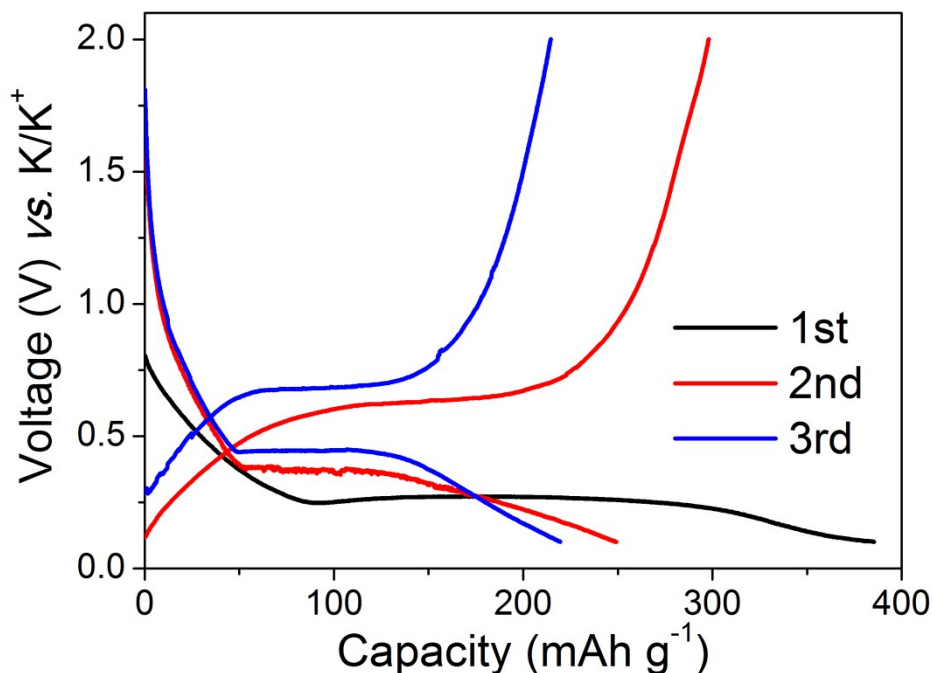


**Figure S15.** Charge-discharge curves of  $K_2TP$  electrode at a current density of  $0.1 \text{ A g}^{-1}$ .  $K_2TP$  electrodes were prepared by mixing  $K_2TP$  with Super P and CMC-Na (5:4:1) in the presence of deionized water and then coated on aluminum sheet using a doctor blade with mass loading of roughly  $1\sim 2 \text{ mg cm}^{-2}$ . The electrodes were dried under vacuum at  $100 \text{ }^\circ\text{C}$  for 12 hrs. The potassium metal was employed as counter electrode and Glass-fiber filter was used as separator. The electrolyte was  $1 \text{ M KPF}_6$  in DME.

## References

1. Y. Wang, Y. Ding, L. Pan, Y. Shi, Z. Yue, Y. Shi and G. Yu, *Nano Lett.*, 2016, 16, 3329-3334.
2. Y. Chen, W. Luo, M. Carter, L. Zhou, J. Dai, K. Fu, S. Lacey, T. Li, J. Wan, X. Han, Y. Bao and L. Hu, *Nano Energy*, 2015, 18, 205-211.
3. Z. Jian, Y. Liang, I. A. Rodríguez-Pérez, Y. Yao and X. Ji, *Electrochem. Commun.*, 2016, 71, 5-8.
4. Q. Zhao, J. Wang, Y. Lu, Y. Li, G. Liang and J. Chen, *Angew. Chem. Int. Ed.*, 2016, 55, 12528-12532.
5. J. Han, G.-N. Li, F. Liu, M. Wang, Y. Zhang, L. Hu, C. Dai and M. Xu, *Chem. Commun.*, 2017, 53, 1805-1808.
6. L. Xue, Y. Li, H. Gao, W. Zhou, X. Lü, W. Kaveevivitchai, A. Manthiram and J. B. Goodenough, *J. Am. Chem. Soc.*, 2017, 139, 2164-2167.
7. H. Kim, J. C. Kim, S. H. Bo, T. Shi, D. H. Kwon and G. Ceder, *Adv. Energy Mater.*, 2017, 7, 1700098.



8. C. Vaalma, G. A. Giffin, D. Buchholz and S. Passerini, *J. Electrochem. Soc.*, 2016, 163, A1295-A1299.
9. J. Liao, Q. Hu, Y. Yu, H. Wang, Z. Tang, Z. Wen and C. Chen, *J. Mater. Chem. A*, 2017, 5, 19017-19024.
10. K. Chihara, A. Katogi, K. Kubota and S. Komaba, *Chem. Commun.*, 2017, 53, 5208-5211.
11. A. Eftekhari, *J. Power Sources*, 2004, 126, 221-228.
12. Y.-H. Zhu, X. Yang, D. Bao, X.-F. Bie, T. Sun, S. Wang, Y.-S. Jiang, X.-B. Zhang, J.-M. Yan and Q. Jiang, *Joule*, 2018, 2, 736-746.
13. Z. Song, T. Xu, M. L. Gordin, Y. B. Jiang, I. T. Bae, Q. Xiao, H. Zhan, J. Liu and D. Wang, *Nano Lett.*, 2012, 12, 2205-2211.